International Journal of Multimedia and Ubiquitous Engineering
Vol.10, No.8 (2015), pp.171-180
http://dx.doi.org/10.14257/ijmue.2015.10.8.17

Detail-Enhanced Medical Image Fusion in NSCT Domain

Guocheng Yang[1,2,3] Leiting Chen [1,3] and Meiling Li [4]

[1]*School of Computer Science and Engineering, University of Electronic Science and Technology of China, Chengdu 611731, China*
[2]*Department of Biomedical Engineering, Luzhou Medical Colleague, Zhongshan Road, Luzhou, Sichuan, 646000, China*
[3]*Provincial Key Laboratory of Digital Media, Chengdu 611731, China*
[4]*School of Life Science and Technology, University of Electronic Science and Technology of China, Chengdu 610054, China*
E-mail:gchyangli@163.com

Abstract

Multimodal medical image fusion technique plays an important role in clinical applications, such as pathologic diagnosis and surgical options. However, many traditional fusion methods cannot well preserve details of source images in the fused image. To address this problem, a detail-enhanced image fusion scheme based on non-subsampled contourlet transform (NSCT) and gain control (i.e., NCGC) is developed in this paper, which can effectively combine the spectral information and the spatial features of source images. The proposed method applies power law transformation to tune coefficients of each decomposed subband, and adjusts the strength of subband signals by smooth gain control. Eventually, the fused image with more anatomical details and functional information is constructed by the inverse NSCT. Three pairs of medical images with different modalities and three fusion metrics are applied to validate the feasibility of this algorithm. Experimental results demonstrate that the proposed method can achieve superior performance in both visual perception and objective assessment.

Keywords: *multimodal medical image fusion; detail-enhanced; non-subsampled contourlet transform; gain control*

1. Introduction

Medical image fusion, as a powerful tool for clinical applications, has been widely developed and plays an important role in medical diagnosis. This technology can capture more spectral information and spatial features in source images, and provide a reliable basis for proper clinical diagnosis and reasonable surgical options. Substantially, it is unrealistic for doctors to obtain comprehensive information from only one single modality image, whereas doctors may attain complementary information from different modality of medical images. For example, the composite image of computed tomography (CT) and magnetic resonance imaging (MRI) can simultaneously provide dense structures like bones and pathological soft tissue information. Similarly, combining single-photon emission computed tomography (SPECT) and MRI image not only visualizes anatomical information, but also provides functional and metabolic information.

With the rapid development of the increasing clinical applications and advanced instrumentations, medical image fusion is widely applied in the areas of medical diagnostics, treatment, assessment, 3D conformal radiotherapy, *etc*. In the past two decades, various effective medical image fusion techniques have been developed, such as independent component analysis (ICA) [1] or principal component analysis (PCA) [2, 3], brovey transform [4], intensity-hue-saturation (IHS) technique [5-7].

ISSN: 1975-0080 IJMUE

The major disadvantages of these fusion methods above are that it introduces spatial distortions in the resultant image and does not provide any spectral information [8]. In addition, image fusion methods based on Pulse coupled neural network (PCNN) are also developed [9-11]. However, one common defect of these schemes is that the whole fusion process cannot finish by one PCNN and more than two PCNNs must be used for fusing multi-source images, resulting in time consuming and inefficient.

Multi-scale decomposition (MSD) based medical image fusion methods have been widely discussed and reported in the literature. In these schemes, the source images are firstly decomposed into low-frequency subband and a set of high-frequency subbands at various scales and directions, then the feasible fusion rules are determined and applied to fuse the high and low frequency subband coefficients. Finally, the fused image is obtained by inverse transform. The typical decomposition methods include laplacian pyramid (LAP) [12], discrete wavelet transform (DWT) [13], wavelet-based statistical sharpness measure (WSSM) [14], morphological difference pyramid (MOD) [15], curvelet transform (CT) [16] and shearlet transform [17, 18], *etc*. Although these fusion methods have achieved good performance in some respects, the fused results are easily accompanied with color distortion or details loss because of low similarity between different modal images.

One of the core problems for MSD-based schemes is the selection of MSD tool. Different transform tools will directly affect the fused outcome. In order to overcome the limitations of the traditional transform tools, some novel multi-scale geometric analysis tools should be fully considered and introduced to medical image fusion. Compared to many existing multi-scale transform tools, the non-subsampled contourlet transform (NSCT) [19] is an over-complete transform, by which, image features at different scales and directions are better captured, which produces resultant image with more details. Based on its perfect image representations, such as fully shift-invariant, multi-scale, and multi-direction expansion, NSCT has been successfully utilized in medical image fusion [20-24].

In this paper, a detail-enhanced multi-modal medical image fusion framework based on NSCT and gain control (NCGC) is developed, which preserves more spatial detail features and more functional information of source images. The research contributions of the paper can be summarized as follows. 1) This paper proposes a new NSCT-domain based fusion framework for multimodal medical images. 2) A novel weight measurements are proposed to compute weight maps for the decomposed subband coefficients. 3) The developed detail-enhanced and brightness-adjusted image fusion method is guided by the power law transformation and smooth gain control map.

The rest of this paper is organized as follows. The proposed fusion framework and the implementation are described in Section 2. Then experimental results and discussion are shown in Section 3. Finally, a conclusion is presented in Section 4.

2. The Proposed Fusion Algorithm

Figure 1 shows the block diagram of the proposed NCGC fusion algorithm. To smoothly combine spectral information (corresponding color image, *i.e*., SPECT/PET) and spatial features (*i.e*., MRI/CT) of source images, the proposed method converts the multispectral image to IHS color space. The independent intensity I component is then decomposed using NSCT and enhanced by a power law transformation. With applying the fusion rule based on the weight map, the decomposed subbands are merged. After that, the blended subbands are further adjusted by gain control. Finally, the resultant image is generated directly by inverse NSCT and inverse IHS transform. It is noted that the fusion procedure will be directly fused without IHS transform when input source images are both gray

images (*e.g.*, CT and MRI). The fusion process is shown as the red bounding box in Figure 1.

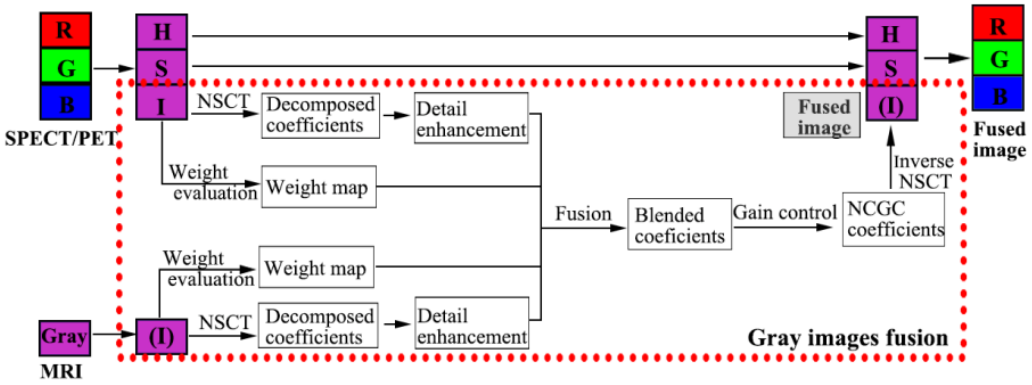

Figure 1. Block Diagram of the Proposed NCGC Fusion Algorithm

2.1. IHS Transform

The IHS transform may be used for fusion of multi-sensor images or medical images [5,25,26], which can convert the multispectral image with red, green and blue channels to intensity, hue and saturation color space effectively. The independent intensity component I representing brightness in a spectrum is less sensitive to noise. Therefore, the fusion of panchromatic image will be better implemented by combining independent intensity component I and high resolution image. Based on this model, the reconstructed image well contains the spatial features with high resolution image (such as MRI) and color information with low resolution multispectral image (such as PET).

The proposed method employs the IHS triangular model [27] to convert the multispectral color image, the conversion system is implemented as the following equations:

$$I = \frac{R+G+B}{3} \tag{1}$$

$$H = \begin{cases} \dfrac{G-B}{3(I-B)} & if \quad B < R,G \\ \dfrac{B-R}{3(I-R)} + 1 & if \quad R < B,G \\ \dfrac{R-G}{3(I-G)} + 2 & if \quad G < R,B \end{cases} \tag{2}$$

$$S = \begin{cases} \dfrac{I-B}{I} & if \quad B < R,G \\ \dfrac{I-R}{I} & if \quad R < B,G \\ \dfrac{I-G}{I} & if \quad G < R,B \end{cases} \tag{3}$$

2.2. Decomposition in NSCT Domain

The implementation of NSCT includes two stages, *i.e.*, non-subsampled pyramid (NSP) and non-subsampled directional filter bank (NSDFB). The former provides multi-scale decomposition and the later provides direction information. The NSP decomposes the original image into a low frequency subband and a high frequency subband at each decomposition stage. Then the NSDFB decomposes the high frequency subband into multiple directional sub-images. Assume that l_j denotes the number of decomposition level at the *j-th* scale in NSCT domain, the high frequency subband produces 2^{l_j} directional sub-images with the same size as the original image. This process also explains why NSCT can capture more precise directional information. For illustration simplicity, with just two input images $I^A(x,y)$ and $I^B(x,y)$ as an example, the decomposition coefficients of the two source images are expressed as $\{ C_{j_0}^A(x,y), C_{j,d}^A(x,y) \}$ and $\{ C_{j_0}^B(x,y), C_{j,d}^B(x,y) \}$. As such, the subband coefficients of the corresponding fused image $I^F(x,y)$ are given by $\{ C_{j_0}^F(x,y), C_{j,d}^F(x,y) \}$. $C_{j_0}^*(x,y)$ denotes the coefficient at the coarsest scale and $C_{j,d}^*(x,y)$ indicates the subband coefficients at the *j-th* scale and direction *d* (*d=1, 2, 3, ...,* 2^{l_j}). In our experiments, the directional decomposition level is [0-2], respectively.

2.3. Detail Enhancement

In this paper, multi-scale contrast str*etc*hing is used to enhance the details of subbands, resulting better contrast and edge sharpness in the reconstructed image. Power law transformation, as one of the most common and basic image enhancement functions, is applied to tune subband coefficients of each decomposition level. The coefficients of the decomposed subband at the *j-th* scale and direction *d* are given as

$$C_{j,d}^{enhanced\_I}(x,y) = \left(C_{j,d}^I(x,y)\right)^{(1-m_d)} \tag{4}$$

Where m_d is a positive and scale-related parameter, which can control the degree of image enhancement.

2.4. Image Fusion

Weight map represents the spatial information of an image objectively, which reveals each pixel's contribution to fusion image at different space position. In this paper, we define the weight map $W_i(x,y)$ using contrast as metrics. Similar to Mertens *et al*. [28], the absolute value after the Laplacian filtering is taken as the contrast indicator. In order to obtain a visually consistent result, weighted maps are smoothed with Gaussian kernel function σ and normalized. As a result, the decomposed subband's weight map is represented as

$$\overline{W_i}(x,y) = \frac{g(\sigma) \otimes W_i(x,y)}{\sum_{i=1}^{N} g(\sigma) \otimes W_i(x,y) + \xi} \tag{5}$$

Where $g(\sigma)$ denotes Gaussian kernel function (σ=5) and *N* is the total number of source images. ξ is a small value (exp(-25)) to avoid singularity.

After obtaining the decomposed subband's weight maps, the fused subband coefficients are calculated by the following forms:

$$C_k^F(x,y) = \sum_{i=1}^{N} \overline{W_i}(x,y) \times C_k^i(x,y) \tag{6}$$

Where $C_k^i(x,y)$ denotes the *k-th* decomposed subband coefficients of the input image $I^i(x,y)$.

2.5. Gain Control

The use of smooth gain control map helps to reduce artifacts and significantly improves the brightness of the subband. This technique has been successfully applied to the scheme of subband enhancement [29], which effectively increase the brightness of subbands and adjust the strength of subband signals, resulting a detail-enhanced composite image. Here is a general description of constructing gain control map. Firstly, an activity map $A_i(x,y)$ can be expressed as (7). Then, similar to [29], gain control map can be derived from the aggregated activity map.

$$A_i(x,y) = g(\sigma) * \left| C_i^F(x,y) \right| \tag{7}$$

$$A_{ag}(x,y) = \sum_{i=1}^{k} g(\sigma) * \left| C_i^F(x,y) \right| \tag{8}$$

$$G_i^{ag}(x,y) = m_i \left(\frac{\varepsilon + A_{ag}(x,y)}{\delta} \right)^{(\gamma-1)} \tag{9}$$

Where, δ and γ is a weighing factor between 0 and 1 (set 0.8), ε (set 0.002) is a small parameter that prevents the noise from being blown up and avoids singularities in the gain control map, α is a constant related to spatial frequency (set 0.2), and $g(\sigma)$ is a Gaussian kernel function. The scale-related parameter m_i controls the modification extent of different frequency, and δ is a gain control stability level that is associated with the activity statistics (with *M* and *N* being the width and height of the subband image) activities closer to δ.

Figure 2 gives the result of applying gain control maps to fuse two medical images. Intuitively, the gain control maps have significant contributions to preserving spatial details of the source images and adjusting the brightness of final image. (c) shows method without gain control does achieve good result, after adjustment with gain control maps, however, a resultant image with more details is obtained in (d). Figure 2(e) is a random scanline of the fused results before and after gain control. The shape of the curve illustrates that the signal is turned up for places where activities are low, which means that the local details and brightness are enhanced by applying gain control maps.

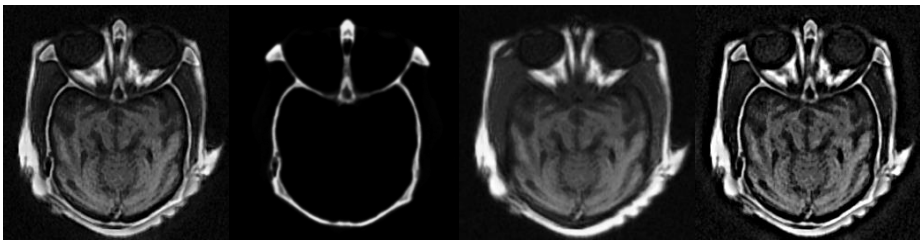

(a) (b) (c) (d)

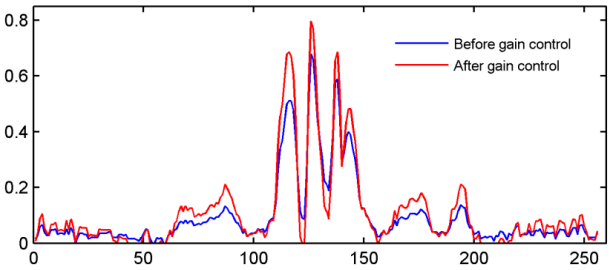

(e)

Figure 2. Comparison of the Fused Results without Gain Control (c) and with Gain Control (d). Source Images CT (a) and MRI (b). (e) Is the Statistical Characters of a Random Scanline in (c) and (d)

3. Experimental Results and Discussion

Three different groups of human brain images are employed to validate the proposed algorithm, including CT/MRI, PET/MRI and SPECT/MRI images. All the images have the size of 256 ×256 pixels, which are already in perfect registration. They can be freely downloaded from the data site (http://www.med.harvard.edu/AANLIB/home.html). The proposed algorithm is compared with the comparative existing fusion methods: the guided filtering based fusion (GFF) [30], WSSM [14], DWT with DBSS (2,2) [13], LAP [12], MOD [15], PCA [3], IHS [7] and pixel averaging fusion method. Like previous studies [30-31], parameters of DWT, LAP, MOD are: decomposition level is set to 3, coefficients fusion rules: selecting max in the high pass and average in the low pass.

Figure 3 shows the results obtained by different fusion methods. As shown in the close-up views of the regions labeled in Figure 4, it can be seen that WSSM and MOD cause serious artifacts in the final image. Relatively, the results from GFF, PCA, Average have some improvement, but they are not enough sharpness. For these methods of DWT, LAP, MOD, although they produced a better effect on bone structures, the texture information is still unclear in soft tissue structures. By contrast, our method NCGC produces a detail-enhanced and brightness-increased resultant image (see (a9)), which simultaneously clearly shows the soft-tissue and bone structures.

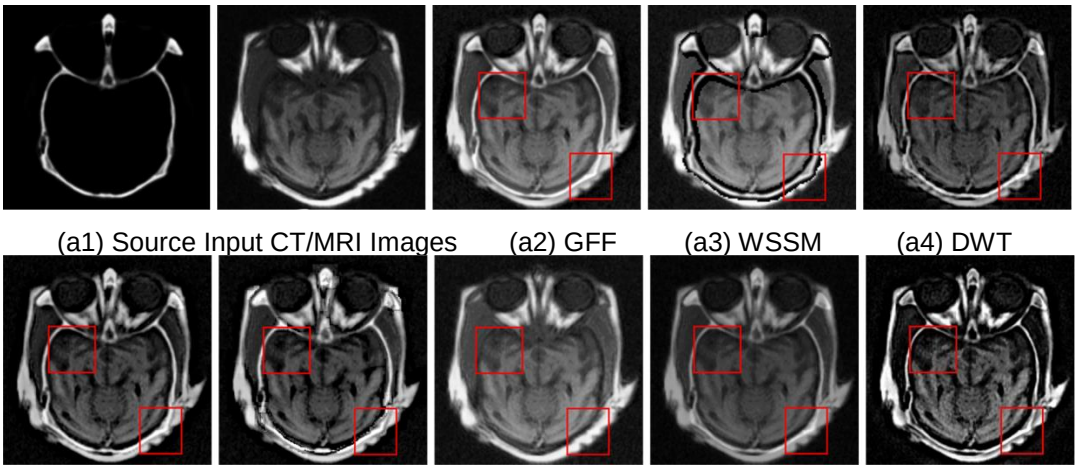

(a1) Source Input CT/MRI Images (a2) GFF (a3) WSSM (a4) DWT

(a5) LAP (a6) MOD (a7) PCA (a8) Average (a9) NCGC

Figure 3. Performance Comparison of different Fusion Methods in CT/MRI

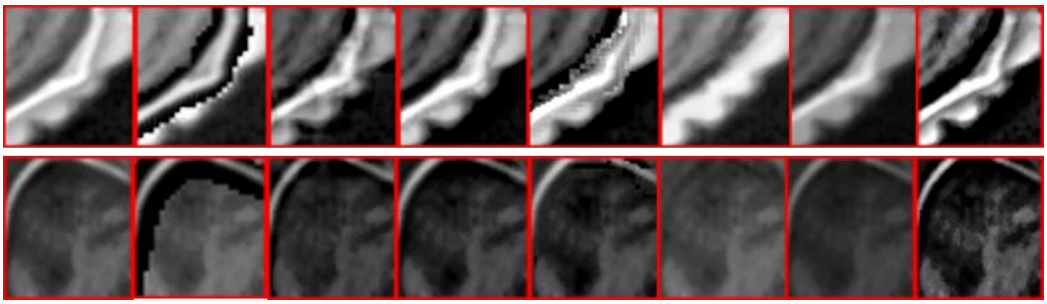

Figure 4. Close-Up Views of the Regions Labeled by the Two Red Rectangles, According to the Order of (a2)~(a9) in Figure 3. The First and Second Row Corresponds to the Upper Left and Lower Right Corner Respectively

Figure 5 and Figure 6 demonstrate the fusion performance between MRI/SPECT image and MRI/PET image, respectively. The two pairs of images are from a man with AIDS dementia and normal coronal of a healthy person, respectively. From Figure 5(b2)-(b9), the result produced by PCA is vague relative to other algorithms and the IHS based method causes serious color distortion. For the two methods, the color information of source SPECT image isn't well transferred to final image (highlighted by green arrows). Although the results that produced by GFF and WSSM are better than the former two methods (PCA, IHS), the local texture information is still unclear. By contrast, the proposed NCGC shows more texture contents and better visual effect in final image, which can be seen from the corresponding regions highlighted by green ellipses. As another example, utilizing MRI and PET images, the fusion results from some typical algorithms are also displayed in Figure 6(c2)-(c9). It can be observed that the spatial features and spectrum information in the original images can be well combined together by the proposed method (c9), in which, the fibrous strands of light matter in the cerebellar lobes are much easier to discern (see the regions labeled by purple ellipses).

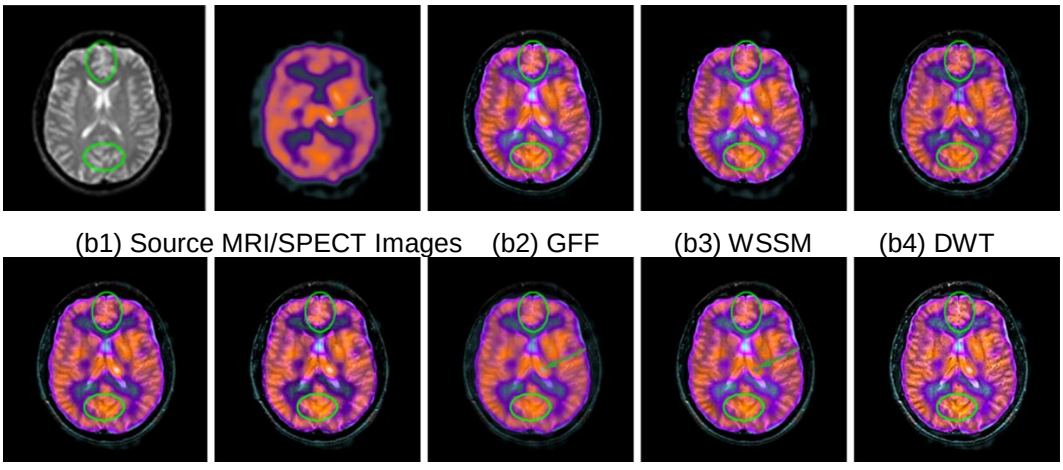

Figure 5. The Fusion Results of MRI and SPECT Images Using Different Fusion Algorithms. (b1) Is Two Source MRI and SPECT Images Respectively

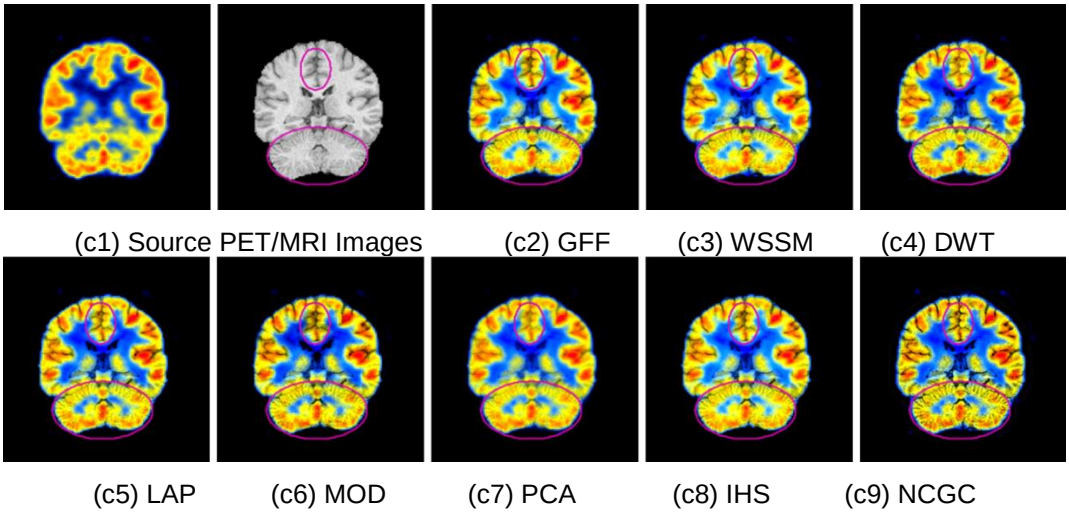

Figure 6. The Fusion Results of the Normal Coronal PET and MRI Images Using Different Fusion Algorithms. (c1) Is Two Source MRI and PET Images Respectively

In order to evaluate the objective fusion performances of different methods, three image fusion quality metrics, *i.e*., average gradient (AG) [32], entropy (EN) and edge intensity (EI) [33] are adopted. Values for these quality indexes are listed in Table 1. The larger AG indicates the better clarity and contrast, the larger EN indicates the richer information and the larger EI indicates the better definition. Table 1 shows the quantitative assessments of the fused images obtained by three different groups of tests, in which, the proposed method gets the largest values to all the metrics. These experimental results demonstrate that the proposed method (*i.e*. NCGC) can well preserve the complementary information of different source images and produce a detail-enhanced image.

Table 1. The Quantitative Assessments of Eight different Fusion Methods

Source Images	Index	GFF	WSSM	DWT	LAP	MOD	PCA	Average/ IHS	Proposed NCGC
Multimodal CT/MRI	AG	6.125	7.727	5.893	6.278	7.085	4.860	3.503	10.700
	EN	6.797	6.215	6.264	6.191	6.263	5.983	5.851	6.837
	EI	66.494	83.346	63.487	67.948	75.940	52.779	38.077	112.83
Multimodal SPECT/MRI	AG	5.404	4.680	5.425	5.390	5.479	3.944	5.440	7.990
	EN	6.080	5.090	6.463	6.091	5.690	5.667	5.097	6.672
	EI	55.495	48.425	55.276	55.018	55.550	41.141	55.835	77.756
Multimodal PET/MRI	AG	5.887	6.020	6.134	6.143	6.132	5.180	5.834	7.786
	EN	5.271	4.682	5.498	5.043	4.964	4.770	4.368	5.634
	EI	61.385	62.827	63.729	63.904	63.482	55.029	63.904	78.390

4. Conclusion and Future Work

In this paper, a novel multimodal medical image fusion method NCGC was developed, which enhances details and adjusts brightness of subbands by power law transformation and smooth gain control maps, respectively. The advantages of the

proposed method are that it can effectively combine the spectral information with the spatial features from the source images, resulting in a visually pleasing and informative composite image. The fused result outperforms the traditional methods in the performance of texture information and brightness, which may help to promote clinical diagnosis. Next step, we will apply a mathematical model to analyze and measure dependencies between different subband coefficients for further improving the fusion performance.

Acknowledgements

The authors would like to thank all the reviewers for giving us their constructive comments and kind suggestions. This work was supported by grants from major special project 2012A090300001, which is integration of enterprises, universities and research institutes in Guangdong province.

References

[1] McKeown M. J., Makeig S., Brown G. G., Jung T. P., Kindermann S. S., Bell A. J. and Sejnowski T. J., "Analysis of fMRI data by blind separation into independent spatial components," DTIC Document, **(1997)**.
[2] Chavez P. T. and Kwarteng A. Y., "Extracting spectral contrast in Landsat Thematic Mapper image data using selective principal component analysis," Photogrammetric Engineering and Remote Sensing, vol. 55 no. 3, **(1989)**, pp.339-348.
[3] Naidu V. and Raol J., "Pixel-level image fusion using wavelets and principal component analysis," Defense Science Journal, vol. 58 no. 3, **(2008)**, pp. 338-352.
[4] Chibani Y., "Additive integration of SAR features into multispectral SPOT images by means of the à trous wavelet decomposition," ISPRS journal of photogrammetry and remote sensing, vol. 60 no. 5, **(2006)**, pp. 306-314.
[5] Tu T. M., Su S. C., Shyu H. C. and Huang P. S., "A new look at IHS-like image fusion methods," Information fusion, vol. 2 no. 3, **(2001)**, pp. 177-186.
[6] Zhang Y. and Hong G., "An IHS and wavelet integrated approach to improve pan-sharpening visual quality of natural colour IKONOS and QuickBird images," Information Fusion, vol. 6 no. 3, **(2005)**, pp. 225-234.
[7] Daneshvar S. and Ghassemian H., "MRI and PET image fusion by combining IHS and retina-inspiredmodels," Information Fusion, vol. 11 no. 2, **(2010)**, pp. 114-123.
[8] Singh R. and Khare A., "Fusion of multimodal medical images using Daubechies complex wavelet transforms-A multiresolution approach," Information Fusion, **(2012)**.
[9] Yang S., Wang M., Jiao L., Wu R. and Wang Z., "Image fusion based on a new contourlet packet," Information Fusion, vol. 11 no. 2, **(2010)**, pp. 78-84.
[10] Jiang H. and Tian Y., "Fuzzy image fusion based on modified Self-Generating Neural Network," Expert Systems with Applications, vol. 38 no. 7, **(2011)**, pp. 8515-8523.
[11] Broussard R. P., Rogers S. K., Oxley M. E. and Tarr G. L., "Physiologically motivated image fusion for object detection using a pulse coupled neural network," Neural Networks, IEEE Transactions on, vol. 10 no. 3, **(1999)**, pp. 554-563.
[12] Burt P. J. and Adelson E. H., "The Laplacian pyramid as a compact image code," Communications, IEEE Transactions on, vol. 31 no. 4, **(1983)**, pp. 532-540.
[13] Mallat S. G., "A theory for multiresolution signal decomposition: the wavelet representation," Pattern Analysis and Machine Intelligence, IEEE Transactions on, vol. 11 no. 7, **(1989)**, pp. 674-693.
[14] Tian J., Chen L., "Adaptive multi-focus image fusion using a wavelet-based statistical sharpness measure," Signal Processing, vol. 92 no. 9, **(2012)**, pp. 2137-2146.
[15] Matsopoulos G., Marshall S. and Brunt J., "Editors. Multiresolution morphological fusion of MR and CT images of the human brain," Vision, Image and Signal Processing, IEE Proceedings; IET, vol. 141 no. 3, June, **(1994)**, pp.137-142.
[16] Ali F., El-Dokany I., Saad A. and Abd El-S. F., "A curvelet transform approach for the fusion of MR and CT images," Journal of Modern Optics, vol. 57 no. 4, **(2010)**, pp. 273-286.
[17] Miao Q. G., Shi C., Xu P. F., Yang M. and Shi Y. B., "A novel algorithm of image fusion using shearlets," Optics Communications, vol. 284 no. 6, **(2011)**, pp. 1540-1547.
[18] Deng C., Wang S. and Chen X., "Editors. Remote sensing images fusion algorithm based on shearlet transform," Environmental Science and Information Application Technology, 2009 ESIAT 2009 International Conference, vol. 3, **(2009)**, pp.451-454.
[19] Da Cunha A. L., Zhou J. and Do M. N., "The non-subsampled contourlet transform: theory, design, and applications," Image Processing, IEEE Transactions on, vol. 15 no. 10, **(2006)**, pp. 3089-3101.

[20] Das S. and Kundu M. K., "NSCT-based multimodal medical image fusion using pulse-coupled neural network and modified spatial frequency," Medical & biological engineering & computing, vol. 50 no. 10, **(2012)**, pp. 1105-1114.
[21] Li T. and Wang Y., "Biological image fusion using a NSCT based variable-weight method," Information Fusion, vol. 12 no. 2, **(2011)**, pp. 85-92.
[22] Savitha V., Kadhambari T. and Sheeba R., "Multimodality Medical Image Fusion Using NSCT," IJREAT International Journal of Research in Engineering & Advanced Technology 1, **(2014)**.
[23] Amini N., Fatemizadeh E. and Behnam H., "MRI-PET image fusion based on NSCT transform using local energy and local variance fusion rules," Journal of medical engineering & technology, vol. 38 no. 4, **(2014)**, pp. 211-219.
[24] Li T. and Wang Y., "Multiscaled combination of MR and SPECT images in neuroimaging: A simplex method based variable-weight fusion," Computer methods and programs in biomedicine, vol. 105 no. 1, **(2012)**, pp. 31-39.
[25] Bhatnagar G., Jonathan W. Q. and Liu Z., "Human visual system inspired multi-modal medical image fusion framework," Expert Systems with Applications, vol. 40 no. 5, **(2013)**, pp. 1708-1720.
[26] Pohl C. and Van G. J., "Review article multisensor image fusion in remote sensing: concepts, methods and applications," International journal of remote sensing, vol. 19 no. 5, **(1998)**, pp. 823-854.
[27] Qiu Z., "The study on the remote sensing data fusion," Acta Geodaetica et Cartographica Sinica, vol. 19 no. 4, **(1990)**, pp. 290-296.
[28] Mertens T., Kautz J. and Van R. F., "Editors. Exposure fusion: A simple and practical alternative to high dynamic range photography," Computer Graphics Forum, **(2009)**.
[29] Li Y., Sharan L. and Adelson E. H., "Editors. Compressing and companding high dynamic range images with subband architectures," ACM Transactions on Graphics (TOG), **(2005)**.
[30] Shutao L., Xudong K. and Jianwen H., "Image Fusion With Guided Filtering," Image Processing, IEEE Transactions on, vol. 22 no. 7, **(2013)**, pp. 2864-2875.
[31] Yong Y., Dongsun P., Shuying H. and Nini R., "Medical image fusion via an effective wavelet-based approach," EURASIP Journal on Advances in Signal Processing, **(2010)**.
[32] Li Z., Jing Z., Yang X. and Sun S., "Color transfer based remote sensing image fusion usingnon-separable wavelet frame transform," Pattern Recognition Letters, vol. 26 no. 13, **(2005)**, pp. 2006-2014.
[33] Yao H., Huseh M. Y., Yao G. and Liu Y., "Image Evaluation Factors. In: Kamel M, Campilho A, editors," Image Analysis and Recognition: Springer Berlin Heidelberg, **(2005)**, pp. 255-262.

